Sodium channel $Na_V1.9$ mutations associated with insensitivity to pain dampen neuronal excitability

Jianying Huang,[1] Carlos G. Vanoye,[2] Alison Cutts,[3] Y. Paul Goldberg,[3] Sulayman D. Dib-Hajj,[1] Charles J. Cohen,[3] Stephen G. Waxman,[1] and Alfred L. George Jr.[2]

[1]Department of Neurology and Center for Neuroscience and Regeneration Research, Yale University School of Medicine; and Rehabilitation Research Center, Veterans Administration Connecticut Healthcare System, West Haven, Connecticut, USA. [2]Department of Pharmacology, Northwestern University Feinberg School of Medicine, Chicago, Illinois, USA. [3]Xenon Pharmaceuticals, Burnaby, British Columbia, Canada.

Voltage-gated sodium channel (Na_V) mutations cause genetic pain disorders that range from severe paroxysmal pain to a congenital inability to sense pain. Previous studies on $Na_V1.7$ and $Na_V1.8$ established clear relationships between perturbations in channel function and divergent clinical phenotypes. By contrast, studies of $Na_V1.9$ mutations have not revealed a clear relationship of channel dysfunction with the associated and contrasting clinical phenotypes. Here, we have elucidated the functional consequences of a $Na_V1.9$ mutation (L1302F) that is associated with insensitivity to pain. We investigated the effects of L1302F and a previously reported mutation (L811P) on neuronal excitability. In transfected heterologous cells, the L1302F mutation caused a large hyperpolarizing shift in the voltage-dependence of activation, leading to substantially enhanced overlap between activation and steady-state inactivation relationships. In transfected small rat dorsal root ganglion neurons, expression of L1302F and L811P evoked large depolarizations of the resting membrane potential and impaired action potential generation. Therefore, our findings implicate a cellular loss of function as the basis for impaired pain sensation. We further demonstrated that a U-shaped relationship between the resting potential and the neuronal action potential threshold explains why $Na_V1.9$ mutations that evoke small degrees of membrane depolarization cause hyperexcitability and familial episodic pain disorder or painful neuropathy, while mutations evoking larger membrane depolarizations cause hypoexcitability and insensitivity to pain.

Introduction

Chronic pain is a prevalent and pernicious medical problem that represents an enormous public health burden. Understanding the molecular mechanisms and identifying critically important proteins involved in nociception may reveal novel therapeutic targets.

Strong evidence supports the contribution of 3 distinct voltage-gated sodium (Na_V) channels ($Na_V1.7$, $Na_V1.8$, and $Na_V1.9$), expressed predominantly in peripheral neurons including pain-signaling neurons, to normal and pathological pain perception (1–6). Whereas $Na_V1.7$ is a fast-gating and tetrodotoxin-sensitive (TTX-S) neuronal Na_V channel, $Na_V1.8$ and $Na_V1.9$ (also known as SNS and NaN, respectively) exhibit TTX resistance (TTX-R) (7–12). $Na_V1.9$ contributes to a persistent sodium current in small-diameter, nociceptive sensory neurons in dorsal root ganglia (DRGs) (13–15) and has been implicated in neuronal pain signaling triggered by inflammation (16–19). These physiological contributions of $Na_V1.9$ may stem from its unique biophysical properties. Specifically, $Na_V1.9$ exhibits voltage dependence of activation and inactivation that overlap near the resting membrane potential (RMP), slow inactivation gating kinetics, and a very large, persistent current (11, 20–24). These properties have been hypothesized to enable $Na_V1.9$ to regulate the threshold for excitability of peripheral nociceptive sensory neurons by modulating both the RMP and responses to subthreshold stimuli (14, 15, 17, 23).

Voltage-gated sodium channels have been implicated in genetic pain disorders by the discovery of mutations in the genes encoding $Na_V1.7$, $Na_V1.8$, and $Na_V1.9$ (1–3, 5, 25, 26). Mutations in $Na_V1.7$ and $Na_V1.8$ have been extensively analyzed, and a clear genotype-phenotype correlation has emerged (2, 27, 28). For $Na_V1.7$, mutations producing gain-of-function biophysical changes at the channel level are associated with disorders of paroxysmal pain (inherited erythromelalgia, paroxysmal extreme pain disorder), whereas those with loss-of-function properties are associated with congenital insensitivity to pain (CIP). Likewise, for $Na_V1.8$, gain-of-function mutations have been identified in subjects with painful peripheral neuropathy. Further, gain-of-function $Na_V1.7$ mutations promote hyperexcitability of DRG neurons in vitro, whereas global knockout of this gene in mice produces the opposite phenotype of insensitivity to pain, with reduced action potential firing in DRG neurons (29), consistent with the increase in threshold of DRG neurons produced by blockade of $Na_V1.7$ (30). This collective work on $Na_V1.7$ and $Na_V1.8$ has established a clear relationship between gain of function at the channel level and severe pain, and channel loss of function and insensitivity to pain, for these 2 channel subtypes.

By contrast, no clear relationship between channel dysfunction and clinical phenotype has yet emerged from early work on $Na_V1.9$ mutations. Mutations of $Na_V1.9$ have recently been associated with

Authorship note: J. Huang and C.G. Vanoye contributed equally to this work.
Conflict of interest: The authors have declared that no conflict of interest exists.
Submitted: December 19, 2016; **Accepted:** March 23, 2017.
Reference information: *J Clin Invest*. 2017;127(7):2805–2814.
https://doi.org/10.1172/JCI92373.

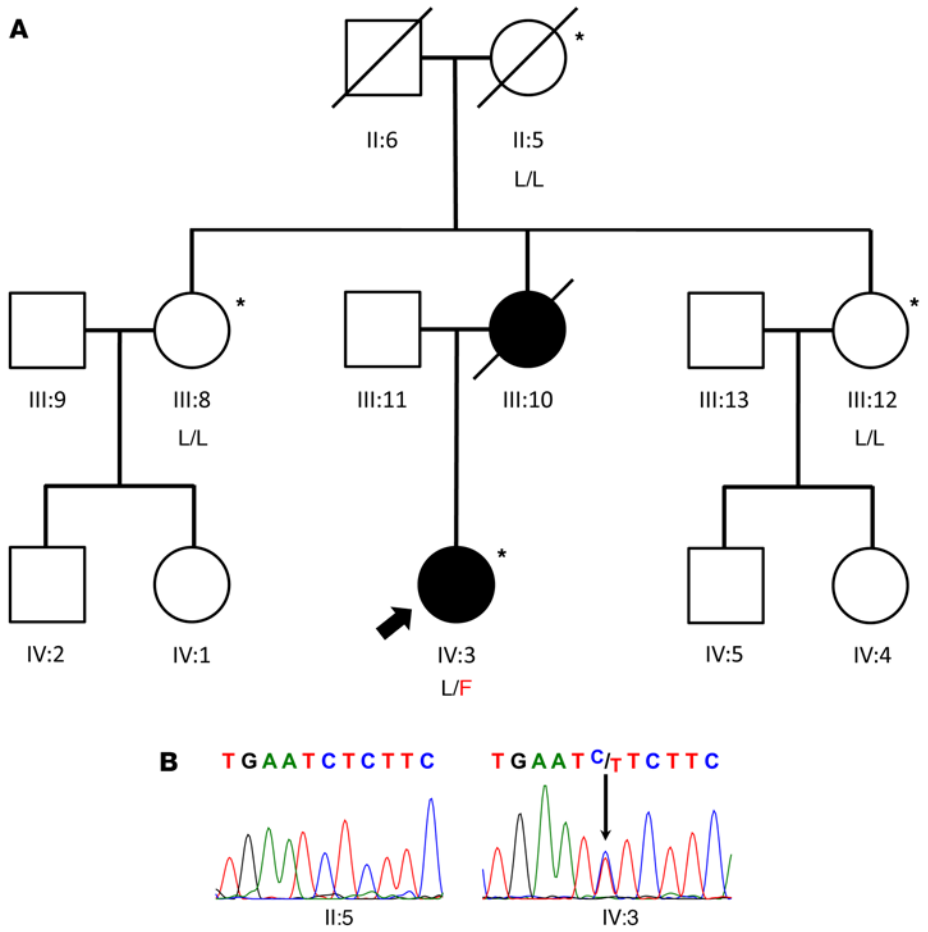

Figure 1. $Na_V1.9$ mutation in a family with insensitivity to pain. (**A**) Three-generation pedigree of the family described in this article. Pedigree symbols define affected (solid), unaffected (open), and deceased (diagonal line) family members. The proband is marked with an arrow. Subjects from whom DNA samples were obtained are marked by asterisks, and genotypes are indicated below pedigree symbols (L/L, homozygous for WT allele; L/F, heterozygous for mutant allele). (**B**) DNA sequence electropherograms demonstrating the L1302F mutation in the proband (IV:3) and WT sequence in the unaffected maternal grandmother (II:5).

either loss of pain perception (26, 31, 32) or the opposite phenotypes of familial episodic pain and painful peripheral neuropathy (33–37). All mutant $Na_V1.9$ channels for which biophysical data are available show hyperpolarizing shifts in channel activation, which is consistent with a gain of function at the channel level, despite the contrasting nature of the associated clinical phenotypes. The physiological basis for this paradox has not been resolved.

In this study, we elucidated the functional consequences of the second $Na_V1.9$ mutation (L1302F) associated with insensitivity to pain and investigated the impact of the 2 known $Na_V1.9$ mutations associated with this condition on the excitability of nociceptive neurons. Our observations demonstrate how these $Na_V1.9$ mutations, which produce a severe gain of function at the channel level, can cause reduced excitability of dorsal root ganglion neurons, consistent with a loss of pain sensibility at the clinical level.

Results

Phenotype and genetics of a proband with insensitivity to pain. We studied a previously described French woman with insensitivity to pain (38). Briefly, both the proband and her mother (Figure 1A) suffered multiple painless orthopedic injuries during childhood including several painless fractures of the lower extremities. Between the ages of 4 and 13 years, the proband suffered a total of 11 fractures, including multiple fractures to both the right and left tibiae. There was radiographic evidence of advanced destruction of the calcaneum and talus. The affected subjects did not perceive a noxious stimulus such as pin-prick as painful and were unable to distinguish a sharp from a blunt object when blinded. Light touch, temperature, and vibration sensations were normal for both affected individuals. Motor nerve conduction velocities were normal for both patients, and nerve fibers were deemed normal upon examination by light and electron microscopy. Motor milestones as well as cognitive and neurological development were normal. The proband reported a normal sense of smell, unlike CIP patients with $Na_V1.7$ mutations, who have anosmia (39, 40). The proband reported severe pruritus since childhood, resulting in painless excoriating lesions of the thorax, ears, and nose from scratching her wounds. She had surgery at age 13 for nasal septum prostheses due to repeated nasal trauma and subsequent deformity. Although the original report on this subject (38) did not document autonomic disturbances, the proband subsequently reported a history of persistent diarrhea of unknown cause as well as episodic abdominal pain beginning in childhood and persisting into adulthood. Sweating was reported as normal.

Targeted sequence analysis of $Na_V1.7$, $Na_V1.8$, and $Na_V1.9$ in the proband identified a heterozygous $Na_V1.9$ coding variant (c.3904C>T, p.Leu1302Phe [L1302F]) (Figure 1B), which was recently reported in an unrelated family with insensitivity to pain (32). The variant affects a highly conserved residue in the S6 segment of domain III and is absent in the Genome Aggregation Database (http://gnomad.broadinstitute.org/). Other family members, including the unaffected maternal grandmother and 2 unaffected maternal aunts, did not harbor the L1302F variant. We

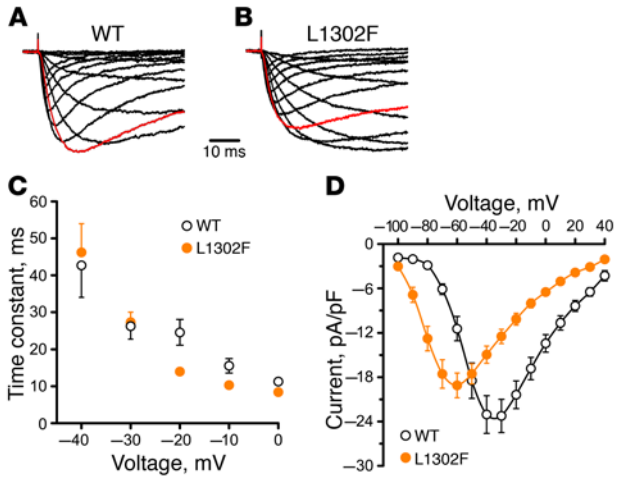

Figure 2. Functional consequences of the $Na_V1.9$ mutation L1302F. Averaged whole-cell sodium currents recorded from ND7/23 cells stably expressing WT (**A**, $n = 17$) or L1302F (**B**, $n = 13$)) $Na_V1.9$ channels. The holding potential was –120 mV. The current traces shown have been normalized to the maximum current amplitude. Red traces indicate whole-cell currents recorded during test depolarizations to –40 mV. (**C**) Voltage dependence of fast inactivation time constants determined from cells expressing WT (black circles) or L1302F (solid orange circles) channels. (**D**) Average current-voltage relationships determined from cells expressing WT (black circles) or L1302F (solid orange circles) channels. Current values were normalized to cell capacitance. Data points in **C** and **D** represent mean values, and error bars indicate the SEM.

presumed that the variant was inherited from the affected mother (deceased), although DNA from the parents was not available to resolve the heritability question. Whole-exome sequencing verified the L1302F variant in the proband, but no other potentially causative variants were discovered in this or other genes with biological plausibility for a genetic pain disorder.

Functional consequences of the $Na_V1.9$ mutation L1302F. To evaluate the functional consequences of the discovered $Na_V1.9$ mutation, we performed a whole-cell voltage-clamp recording of ND7/23 cells stably transfected with WT or mutant human $Na_V1.9$ channels. Figure 2, A and B, illustrates the average TTX-R whole-cell currents for WT and L1302F channels. The inactivation kinetics were similar (Figure 2C), but peak activation of mutant channels occurred at more hyperpolarized test potentials (Figure 2D). Cells expressing WT $Na_V1.9$ exhibited a whole-cell current that peaked at approximately –40 mV, whereas L1302F current densities peaked at approximately –65 mV. The peak current density was not significantly different between cells expressing WT or L1302F (Figure 2D and Table 1).

The L1302F mutation has a significantly hyperpolarized (–26.9 mV shift) voltage dependence of activation (Table 1) and a significantly steeper slope (Table 1) compared with WT channels (Figure 3A). By contrast, the voltage dependence of inactivation following a 300-ms prepulse was not different between WT and L1302F channels (Figure 3B and Table 1), but the slope factor was significantly different (Table 1). The steady-state inactivation and conductance voltage (activation) curves for WT sodium currents intersected near –50 mV, while those for L1302F intersected around –70 mV (Figure 3C). The hyperpolarized shift in activation voltage dependence, without a concomitant shift in the voltage dependence of inactivation observed for L1302F, creates an expanded range of membrane potentials at which channels will be conducting (window current). The physiological impact of this finding would be predicted to be the potentiation of channel activity at or near the resting potential or nociceptive DRG neurons.

Effects of mutant $Na_V1.9$ on DRG neuron excitability. To assess the effect of $Na_V1.9$ mutations on DRG neuron excitability, we performed current-clamp recordings in small (<30 μm) rat DRG neurons electroporated with WT or L1302F channels. $Na_V1.9$ is known to contribute to a depolarizing effect on the resting membrane potential (RMP) (23, 41), and we expected that the enhanced window current of L1302F would potentiate this effect. Consistent with this expectation, we observed that expression of L1302F evoked a marked depolarization of the average RMP by 11.5 mV as compared with WT channel expression in small DRG neurons (Figure 4A and Table 2). All neurons expressing WT $Na_V1.9$ fired action potentials, with an average current threshold of 290 ± 38 pA (Figure 4B and Table 2). A representative action potential from a neuron expressing WT $Na_V1.9$ channels evoked when the current injection reached 280 pA is shown in Figure 4B. The RMP for this neuron was –57.2 mV. By contrast, 4 of 32 (13%) neurons expressing L1302F were unable to fire action potentials in response to stimuli applied at their native resting potentials. All nonfiring L1302F-expressing cells exhibited markedly depolarized RMP values (Figure 4A, solid orange circles).

Because we expected that the depolarized RMP would contribute to the effect of the mutant channel on DRG neuron excitability, we imposed a relatively normal membrane potential in cells expressing these mutant channels by injecting a hyperpolarizing current to achieve a holding potential of –60 mV. All 4 of these cells regained excitability when held at –60 mV and either fired spontaneously or produced overshooting action potentials with threshold currents of 40 pA, 55 pA, and 110 pA, respectively. As an example, a cell recorded at its native RMP of –26.6 mV (solid orange circle indicated by the arrow in Figure 4A) failed to produce an action potential with stimuli as large as 500 pA applied from this resting potential (Figure 4C), whereas the cell fired an action potential at a threshold current as low as 40 pA when held at –60 mV (Figure 4D).

We observed similar phenomena in neurons transfected with L811P, which was previously associated with insensitivity to pain (26). Small DRG neurons expressing L811P exhibited an 8.2-mV depolarized RMP, a smaller effect than was observed for

Table 1. Functional properties of WT and mutant human $Na_V1.9$ channels

	Peak current density (pA/pF)	Voltage dependence of activation $V_{1/2}$ (mV)	k	Voltage dependence of inactivation $V_{1/2}$ (mV)	k
WT	–23.4 ± 2.2 ($n = 17$)	–54.2 ± 1.3 ($n = 17$)	7.1 ± 1.3	–55.3 ± 2.3 ($n = 8$)	8.1 ± 0.5
L1302F	–19.1 ± 1.7 ($n = 13$)	–81.2 ± 1.3 ($n = 13$)[B]	5.6 ± 0.3[B]	–51.1 ± 3.6 ($n = 7$)	16.1 ± 3.0[A]

[A]$P < 0.05$ and [B]$P < 0.001$, by t test compared with WT values.

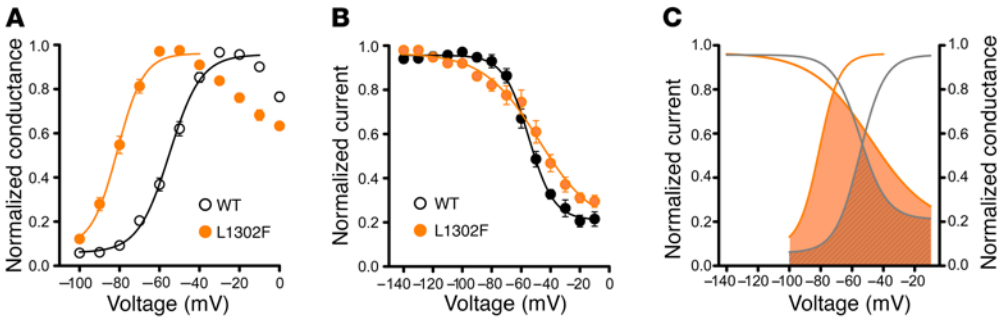

Figure 3. Effects of L1302F on voltage dependences of activation and inactivation. (**A**) Voltage dependence of activation determined for sodium currents recorded from ND7/23 cells stably expressing WT (black circles, n = 17) or L1302F (solid orange circles, n = 13) $Na_V1.9$ channels. (**B**) Voltage dependence of inactivation calculated for currents recorded from ND7/23 cells stably expressing WT (black circles, n = 8) or L1302F (solid orange circles, n = 7) $Na_V1.9$ channels. In both **A** and **B**, the solid lines represent Boltzmann fits to averaged data. (**C**) Superimposed steady-state inactivation and activation curves calculated for WT (gray lines) and L1302F (orange lines) sodium currents. The steady-state inactivation and activation curves for WT intersect near –50 mV, while those for L1302F intersect at approximately –70 mV. Shaded areas indicate the window current between –100 and –10 mV, with the solid orange-shaded area representing the window current for L1302F channels and the hatched area indicating the window current for WT channels. Data points in **A** and **B** represent mean values, and error bars indicate the SEM.

L1302F (Table 2 and Figure 4E). As indicated by the solid purple diamonds in Figure 4E, 8.7% of neurons (4 of 46 cells) expressing L811P were nonexcitable at their native RMP. When held at –60 mV, however, all 4 cells fired spontaneously. Figure 4F illustrates representative spontaneous firing in the cell (indicated by the arrow in Figure 4E) recorded continuously for 30 seconds, with no external stimuli.

We posited that RMP depolarizations evoked by expression of L1302F or L811P caused inactivation of voltage-gated sodium channels, including $Na_V1.8$, which contributes substantially to the action potential upstroke (42). This effect is predicted to attenuate action potential amplitude in neurons that do fire and to completely impair action potential generation in the most severely depolarized neurons expressing mutant $Na_V1.9$ channels. A comparison of spontaneous action potential waveforms among cells expressing WT or mutant channels is shown in Figure 5A, which depicts a marked depolarization of the RMP and an attenuated overshoot in cells expressing either L1302F or L811P.

We previously demonstrated that the action potential amplitude in small adult mouse DRG neurons decreases as the membrane potential is depolarized from –90 mV to –30 mV and that this amplitude–membrane potential relationship depends on the activity of both TTX-S and TTX-R (e.g., $Na_V1.8$) sodium channels (43). Consistent with the hypothesis that a lower action potential amplitude is due to inactivated Na_V channels, we observed that the action potential amplitude was attenuated significantly in cells expressing L1302F and L811P at their native resting potentials (Table 2) but was rescued by holding cells at –60 mV (Table 3). The magnitude of the reduction in action potential amplitude by L1302F (20%) was greater than that for L811P (8.5%), paralleling the larger RMP depolarization in cells expressing L1302F (11.5 mV for L1302F versus 8.2 mV for L811P; Table 2).

Because it is difficult to measure the responses to injected current in spontaneously firing neurons, we excluded them from the analysis of RMP, input resistance, and amplitude of action potential. We did not observe a difference in the percentage of cells expressing L1302F or L811P that fired spontaneously at the native RMP as compared with cells expressing WT channels (Table 2). However, cells expressing L1302F or L811P showed a significantly higher proportion of spontaneously firing cells than did WT cells when using a holding potential of –60 mV (Table 3, and Figure 5B). These observations are consistent with the conclusion that, at the channel level, mutations confer a gain of function, which evokes neuronal hyperexcitability at a physiological RMP.

Input resistance was significantly smaller in DRG neurons expressing L1302F than in cells expressing WT channels at both the native RMP and when held at –60 mV (Tables 2 and 3). Neu-

Table 2. Electrophysiological properties of small DRG neurons expressing WT or mutant $Na_V1.9$ measured at native resting membrane potentials

	Resting membrane potential (mV)	Nonfiring cells (%)	Input resistance (MΩ)	Current threshold (pA)	AP amplitude (mV)
Comparison of WT and L1302F					
WT	–52.7 ± 0.89 (n = 32)	0/32 (0%)	535 ± 54 (n = 32)	290 ± 38 (n = 32)	107 ± 1.9 (n = 32)
L1302F	–41.2 ± 1.5[C] (n = 32)	4/32 (13%)[A]	353 ± 39[B] (n = 28)	243 ± 37 (n = 28)	85.7 ± 3.4[C] (n = 28)
Comparison of WT and L811P					
WT	–53.4 ± 0.57 (n = 51)	0/51 (0%)	555 ± 37 (n = 51)	236 ± 27 (n = 51)	106 ± 1.5 (n = 51)
L811P	–45.2± 1.4[C] (n = 46)	4/46 (8.7%)[A]	465 ± 35 (n = 42)	188 ± 26 (n = 42)	97 ± 2.3[C] (n = 42)

[A]P < 0.05, by z test compared with WT values; [B]P < 0.01 and [C]P < 0.001, by t test compared with WT values. AP, action potential.

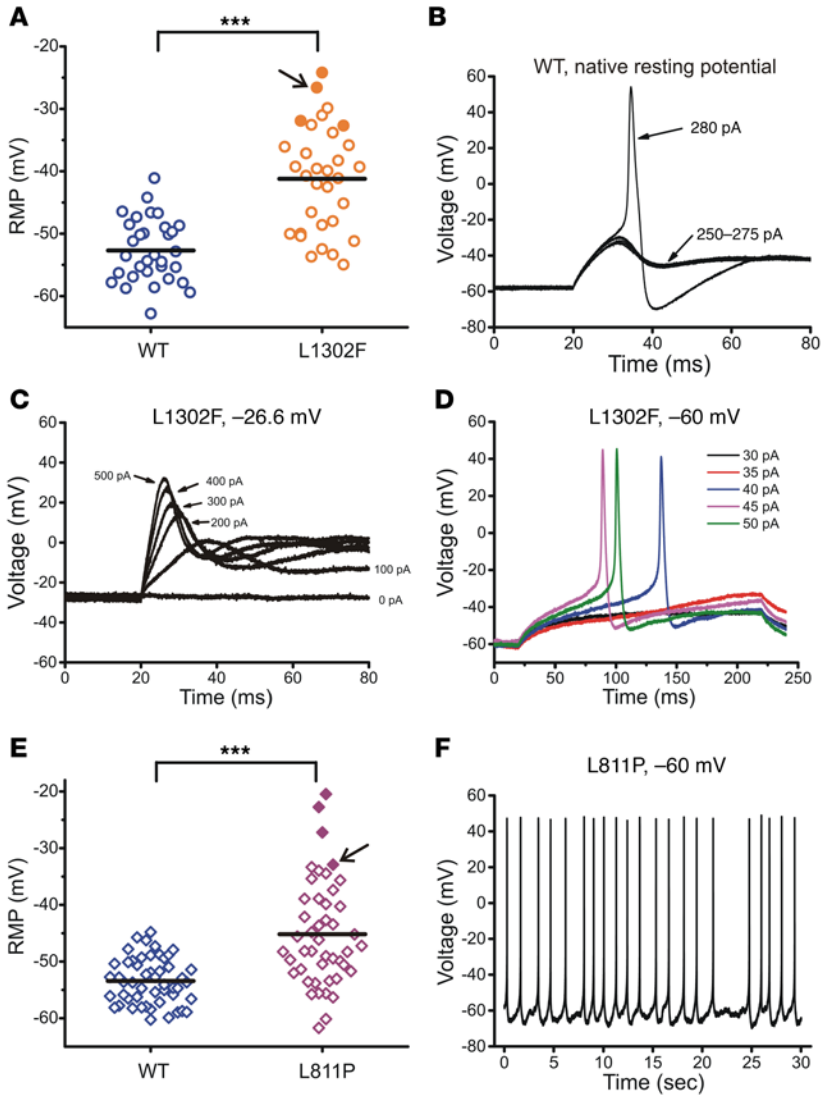

Figure 4. Effects of mutant channels on the RMP in small DRG neurons. (**A**) Scatter-plot of the RMP recording from neurons expressing either WT or L1302F $Na_V1.9$ channels. ***$P < 0.001$, by t test. Solid orange circles indicate cells that did not fire all-or-none action potentials in response to external stimuli at their native resting potentials (–24.2 mV, –26.6 mV, –31.9 mV, and –32.7 mV, respectively) but regained excitability when held at –60 mV. (**B**) Representative action potential in a small DRG neuron overexpressing WT channels evoked when the current injection reached 280 pA. The native resting potential for this neuron was –57.2 mV. (**C**) Small DRG neuron with a RMP of –26.6 mV (indicated by an arrow in panel A) did not fire action potentials in response to 200-ms current injections from 0 to 500 pA in 100-pA increments. (**D**) When held at –60 mV, the same neuron as that depicted in C produced subthreshold depolarizations in responses to 30-pA and 35-pA current injections and generated action potentials with a threshold current of 40 pA. (**E**) Scatter-plot of the RMP in neurons overexpressing either WT or L811P $Na_V1.9$ channels. ***$P < 0.001$, by t test. Four cells indicated by solid purple diamonds did not fire action potentials in response to external stimuli at their native resting potentials (–20.5 mV, –22.7 mV, –27.2 mV, and –32.9 mV, respectively), but fired spontaneously when held at –60 mV (illustrated in panel **F**). The cell indicated by the arrow had a RMP of –32.9 mV. (**F**) Representative spontaneous firing from a holding potential of –60 mV recorded from the cell marked by an arrow in **E**.

rons expressing L811P also exhibited a significantly lower input resistance at –60 mV, but input resistance measured at the native RMP was not significantly different (Table 3). Lower input resistance, also consistent with a gain of function at the channel level, can be attributed to the large conductance of L1302F and L811P channels at negative potentials owing to the hyperpolarized voltage dependence of activation.

Whereas all cells expressing WT $Na_V1.9$ channels fired action potentials when assessed at the native RMP, 13% of cells expressing L1302F and 8.7% of cells expressing L811P did not fire at the native RMP (Table 2). In an analysis in which we excluded spontaneously firing cells, the current threshold was significantly smaller in L1302F-expressing neurons when held at –60 mV (Table 3), presumably due to the relief of resting sodium channel inactivation, while the current threshold was not significantly different in cells expressing L811P (Table 3). However, if spontaneously firing cells were included in this analysis, then the current threshold determined for both L1302F and L811P was significantly smaller than the threshold for WT-expressing cells (Table 3).

Impact of RMP depolarization on current threshold and action potential amplitude. Expression of either L1302F- or L811P-mutant channels produced large RMP depolarizations in small DRG neurons. To model the effect of this depolarization on neuron excitability, we examined nontransfected adult rat DRG neurons within 8 hours of isolation using whole-cell current-clamp recording. Inward currents were injected to clamp the membrane potential at a series of voltages from –60 mV to –30 mV in 2.5-mV increments. This experiment demonstrated that the current threshold for action potential generation falls in direct relationship to the extent of membrane depolarization until a critical point, at which further depolarization requires larger stimuli to initiate a response, is reached (Figure 6A). This U-shaped curve is similar to the relationship between current threshold and resting potential predicted from studies in which the membrane potential was modulated by injections of hyperpolarizing and depolarizing current more centrally along the somatosensory pathway in rat dorsal column axons (44).

This relationship provides an explanation for why large depolarizations caused by expression of L1302F (11.5 mV) or L811P (8.2 mV) are associated with hypoexcitability, whereas lesser degrees of membrane depolarization, which are evoked by other $Na_V1.9$ mutations associated with familial episodic pain disorder or pain-

Table 3. Electrophysiological properties of small DRG neurons expressing WT or mutant $Na_V1.9$ (holding potential of –60 mV)

	Spont. firing cells (%)	Input resistance (MΩ)	Current threshold excl. spont. firing cells (pA)	Current threshold incl. spont. firing cells[A] (pA)	AP amplitude (mV)
			Comparison of WT and L1302F		
WT	0/24 (0%)	519 ± 55 (*n* = 19)	284 ± 44 (*n* = 24)	284 ± 44 (*n* = 24)	116 ± 1.9 (*n* = 24)
L1302F	7/30 (23%)[B]	374 ± 30[D] (*n* = 21)	139 ± 31[D] (*n* = 23)	106 ± 26[F] (*n* = 30)	108 ± 2.7[D] (*n* = 23)
			Comparison of WT and L1302F		
WT	2/56 (3.6%)	504 ± 27 (*n* = 54)	226 ± 24 (*n* = 54)	218 ± 24 (*n* = 56)	116 ± 0.90 (*n* = 54)
L811P	30/60 (50%)[C]	417 ± 31[D] (*n* = 30)	239 ± 37 (*n* = 30)	120 ± 24[E] (*n* = 60)	113 ± 1.7 (*n* = 30)

[A]Current threshold for spontaneously firing cells was assigned a value of 0 pA; [B]$P < 0.05$ and [C]$P < 0.001$, by *z* test compared with WT values; [D]$P < 0.05$, [E]$P < 0.01$, and [F]$P < 0.001$, by *t* test compared with WT values. incl., including; excl., excluding; Spont., spontaneously.

ful neuropathy, cause neuronal hyperexcitability. The representative action potential traces recorded from nontransfected DRG neurons at different clamping voltages (–60 mV, –52.5 mV, –42.5 mV, and –40 mV) shown in the bottom panel of Figure 6A further validate this conclusion. The relationship between action potential amplitude and the extent of RMP depolarization is best fit by a Boltzmann function having a midpoint voltage (–38.7 ± 2.3 mV; Figure 6B) that is close to the midpoint voltage for fast inactivation of $Na_V1.8$, which contributes a major component of the inward current underlying the action potential upstroke, and is consistent with the midpoint voltage (–37 mV) determined previously for TTX-R current in DRG neurons (43).

Discussion

Syndromes of insensitivity to pain have been associated with mutations of 2 voltage-gated sodium channels, $Na_V1.7$ and $Na_V1.9$. In the case of $Na_V1.7$, a sodium channel that sets the gain on nociceptive DRG neurons (30, 45, 46), the congenital inability to sense pain is associated with recessive mutations that produce loss of function at the channel level (39, 47, 48). By contrast, dominant $Na_V1.7$ mutations that produce gain-of-function changes, including a hyperpolarizing shift in the voltage dependence of activation at the channel level, are associated with genetic disorders featuring increased pain sensation (49–52). Unlike the distinct relationships between channel defects and clinical phenotypes for $Na_V1.7$, dominant mutations that produce gain of function in $Na_V1.9$ at the channel level have been associated with syndromes characterized by both insensitivity to pain (26, 31) and severe pain (6, 33, 34, 36). The mechanistic link between $Na_V1.9$ gain of function and insensitivity to pain has been elusive.

The results of our functional profiling provide a mechanistic explanation for a loss of pain sensibility in these patients. Specifically, our voltage-clamp studies revealed a large hyperpolarizing shift in the voltage dependence of activation for L1302F (–26.9 mV) that was qualitatively similar to the results reported for the L811P mutation (26). This biophysical effect causes a larger window of overlap between the voltage dependence of activation and steady-state inactivation (Figure 3C), and this phenomenon is expected to promote large depolarizing current near the RMP in DRG neurons carrying these mutations. Consistent with this prediction, we observed large depolarizations in the average resting potential (11.5 mV for L1302P, and 8.2 mV for L811P) in DRG neurons transfected with either mutation, with resulting impairments in action potential generation.

To examine the effect of this depolarization on excitability, we assessed the effect of holding potential on current threshold in non-

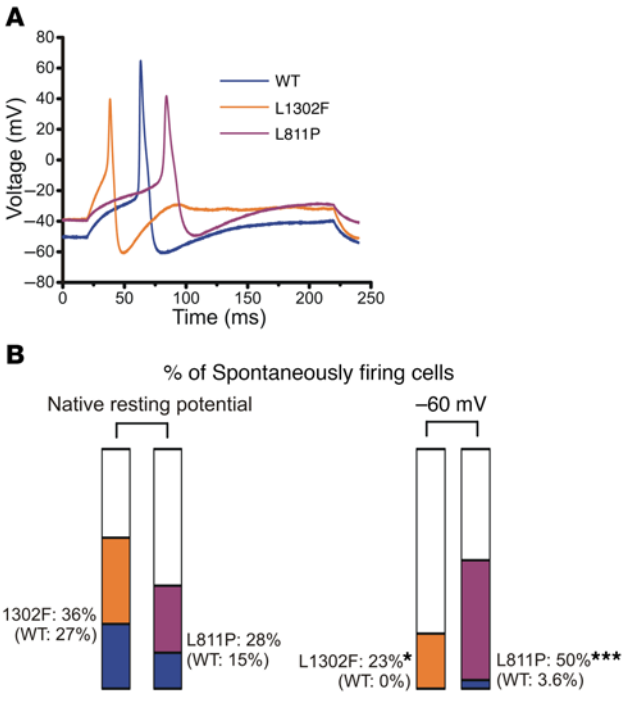

Figure 5. Effects of mutant channels on action potential properties. (**A**) Representative recordings demonstrating that expression of L1302F (orange trace) and L811P (purple trace) was associated with a depolarized RMP and an attenuated action potential overshoot as compared with cells expressing WT channels (blue trace). (**B**) Proportions of spontaneously firing cells. Colors represent the percentage of spontaneously firing cells for WT (blue), L1302F (orange), and L811P (purple) when studied at the native RMP or when using a holding potential of –60 mV. The plotted data sets for the native RMP were L1302F: 18 of 50 cells (36%) versus WT: 12 of 44 cells (27%), $P = 0.35$, by *z* test, and L811P: 18 of 64 cells (28%) versus WT: 9 of 60 cells (15%), $P = 0.079$, by *z* test. When cells were held at –60 mV, 23% of cells expressing L1302F (7 of 30) as opposed to 0% of cells expressing WT fired spontaneously (*$P = 0.012$, by *z* test), whereas 50% of cells expressing L811P (30 of 60) fired spontaneously as compared with 3.6% (2 of 56) of cells expressing WT (***$P < 0.0001$, by *z* test).

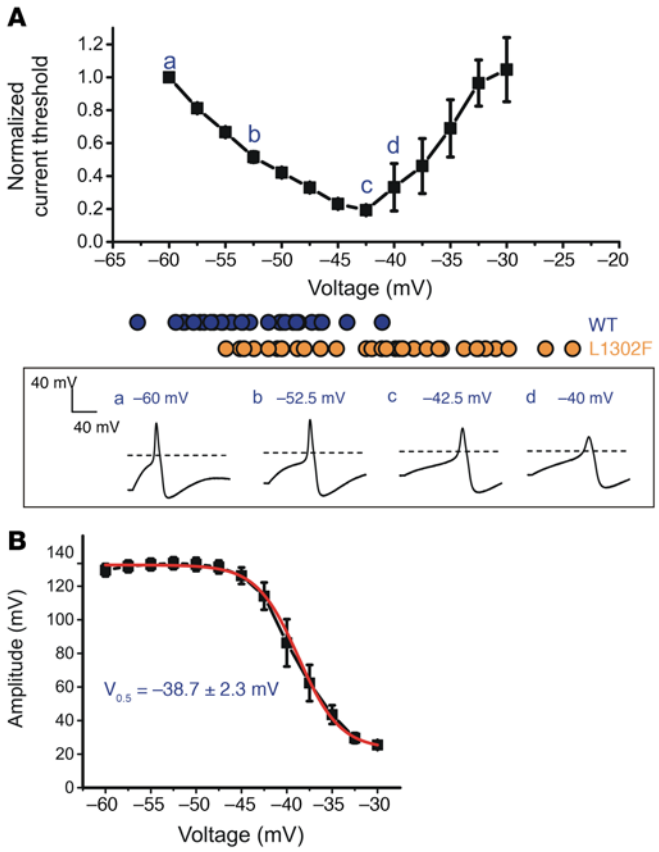

Figure 6. Depolarization of RMP causes biphasic changes in the current threshold and attenuates the action potential amplitude. Small adult DRG neurons were held at membrane potentials ranging from –60 mV to –30 mV in 2.5-mV increments. The RMP distribution in WT- and L1302F-expressing neurons is illustrated by blue (WT) and orange (L1302F) solid circles. Action potential waveforms recorded at various voltages from representative cells are illustrated in the boxed panel below. (**B**) Action potential amplitude and resting membrane potential data were best fit by a single Boltzmann function with a midpoint voltage of –38.7 ± 2.3 mV. Data points in **A** and **B** represent mean values (n = 5), and error bars indicate the SEM.

transfected adult rat DRG neurons. This experiment demonstrated that the current threshold for action potential generation decreases gradually with membrane depolarization until a critical point, at which further depolarization requires larger stimuli to initiate a response, is reached. Notably, when we injected current into nontransfected cells to produce membrane depolarizations similar to those caused by expression of L1302F (+11.5 mV) or L811P (+8.2 mV), we observed a reduced ability to fire action potentials. These findings are in contrast to our previous observations that a 4- to 6-mV depolarization in the resting potential of DRG neurons associated with multiple $Na_V1.9$ as well as $Na_V1.7$ mutations results in neuronal hyperexcitability and paroxysmal pain disorders (27, 34, 53–55). These divergent observations regarding the effects of mutations on neuronal excitability are explained by the U-shaped relationship between resting potential and current threshold (Figure 6A), which demonstrates hyperexcitability of neurons with a moderately depolarized RMP and hypoexcitability of neurons with a severely depolarized RMP.

An explanation at the channel level for how depolarization induced by L1302F or L811P expression leads to hypoexcitability is provided by our observation that a reduction in action potential amplitude is correlated with the degree of RMP depolarization, with a relationship suggesting involvement of $Na_V1.8$ channels, which produce most of the inward current underlying action potential upstroke (43, 56). This conclusion is based on earlier studies, in which we found that the action potential amplitude in small DRG neurons decreases as the membrane potential is depolarized from –90 mV to –30 mV (43). The relationship between membrane potential and action potential amplitude was best fit by 2 Boltzmann equations having voltage for half-maximal channel activation values ($V_{1/2}$) of –73 and –37 mV, matching the $V_{1/2}$ values for steady-state fast inactivation of TTX-S ($Na_V1.7$) and TTX-R ($Na_V1.8$) sodium channels, respectively, and pointing to inactivation of these channels as critical for action potential amplitude. Consistent with these earlier findings, we observed here that the action potential amplitude was attenuated significantly (P < 0.001, Table 2) in DRG neurons expressing L1302F and L811P at their native resting potentials, but the ability to fire full, overshooting action potentials was restored when membrane potentials in these neurons were set to –60 mV, reversing Na_V inactivation.

Impaired excitability of nociceptor neurons was also observed in mice with an engineered murine $Na_V1.9$ mutation (L799P) analogous to human $Na_V1.9$-L811P, but a different interpretation of the mechanisms responsible for this effect was offered (26). Specifically, Leipold and colleagues argued for a conduction block secondary to inactivation of $Na_V1.7$, $Na_V1.8$, and neuronal calcium channels as the central basis for impaired nociception (26). By contrast, our data support a primary loss of neuronal excitability as a direct consequence of a massively depolarized RMP, with some cells displaying a RMP more depolarized than –35 mV (Figure 4E), a voltage domain where there is clear hypoexcitability of DRG neurons. We would also note that mutant channel behaviors reported in the earlier study differ between human $Na_V1.9$-L811P and mouse $Na_V1.9$-L799P, which is not surprising, given the poor conservation of these orthologous proteins (e.g., 73% amino acid identity) relative to other mammalian sodium channels. Although both human and mouse mutations evoke a similar hyperpolarized activation voltage dependence, there were notable differences in the time course of inactivation, sodium current density, and voltage dependence of inactivation (26), all of which confound direct comparisons and diminish the reliability of extrapolating across species.

Some parallels can be drawn between the divergent cellular effects of $Na_V1.9$ gain-of-function mutations and those of the skeletal muscle channel $Na_V1.4$, mutations, which are associated with genetic disorders of muscle contraction (57, 58). Gain-of-function $Na_V1.4$ mutations predominantly cause myotonia or periodic paralysis, symptoms that represent either enhanced or diminished sarcolemmal excitability, respectively. This spectrum of pathophysiological effects has been attributed to specific mechanisms of channel dysfunction and the manner by which dysfunctional channels affect the resting potential. Mutations that impair fast inactivation typical of myotonic disorders promote hyperexcitability by increasing sodium channel availability and by prolonging the muscle action potential, which promotes greater t-tubular potassium accumulation and a greater probability of after-depolarizations. By contrast, an enhanced persistent

sodium current (59, 60) or an anomalous gating pore current (61, 62) typical of mutations associated with either hyperkalemic or hypokalemic periodic paralysis, respectively, causes sustained depolarization of the resting potential and inexcitability owing to inactivation of WT sodium channels. The cellular effects of $Na_V1.9$ mutations associated with insensitivity to pain are most reminiscent of the behavior of $Na_V1.4$ in hyperkalemic periodic paralysis, in that abnormal sodium conductance renders the membrane depolarized and inexcitable.

In conclusion, we determined that large hyperpolarizing shifts in the voltage dependence of activation in mutant $Na_V1.9$ channels associated with insensitivity to pain evoke a degree of membrane depolarization that renders DRG neurons hypoexcitable, probably because of inactivation of other peripheral nerve sodium channels (including $Na_V1.8$). Thus, our observations provide a mechanistic explanation for loss of pain sensibility associated with $Na_V1.9$ mutations that exhibit severe gain of function at the channel level.

Methods

Study subject and molecular genetics. A French proband with insensitivity to pain and her family were recruited as part of a larger study to investigate the molecular basis of loss of sensitivity to pain. At age 33, the proband was enrolled in our study, at which time an updated medical history was collected from the patient's self-reports. Genetic studies included Sanger sequencing of SCN9A (NaV1.7), SCN10A ($Na_V1.8$), and SCN11A ($Na_V1.9$). Subsequently, whole-exome sequencing was performed using the SureSelect V4 Capture Reagent (Agilent Technologies), followed by 80× on-target sequencing using a HiSeq 2000 Sequencer (Illumina).

Plasmids and cell transfection. The L811P and L1302F mutations were introduced into full-length human $Na_V1.9$ (GenBank accession number NP_0554858.2) cDNA including a C-terminal triple FLAG epitope as previously described (22). All recombinant cDNAs were sequenced in their entirety to confirm the presence of the intended modifications and the absence of unwanted mutations.

Heterologous expression experiments were conducted using ND7/23 cells (Sigma-Aldrich) grown at 37°C with 5% CO_2 in DMEM supplemented with 10% FBS (Atlanta Biologicals), 2 mM L-glutamine, and penicillin/streptomycin (50 units/ml and 50 μg/ml, respectively). Unless otherwise stated, all tissue culture media were obtained from Life Technologies (Thermo Fisher Scientific).

Stable expression of mutant $Na_V1.9$ channels in ND7/23 cells (Sigma-Aldrich) was achieved using the piggyBac transposon system as previously described (63, 64) using a transposon vector containing a puromycin resistance gene (pB-$Na_V1.9$_mut-3xFLAG-PuroR). ND7/23 cells were cotransfected with a NaV1.9 plasmid and pCMV-hyPBase encoding a hyperactive version of the piggyBac transposase (65) using FUGENE-6 (Roche Applied Science). Stable $Na_V1.9$-expressing cells were selected with puromycin (3 g/ml; Gibco, Invitrogen, Thermo Fisher Scientific), and individual cell colonies were isolated by limiting dilution. The ND7/23 cell line stably expressing human WT $Na_V1.9$ was previously reported (22).

Voltage-clamp electrophysiology. Cells stably expressing $Na_V1.9$ were incubated at 28°C with 5% CO2 for approximately 24 hours before their use in electrophysiology experiments. Cells were dissociated by trituration, resuspended in supplemented DMEM medium (without puromycin), plated on glass coverslips, and allowed to recover for approximately 2 hours (1 h at 37°C, and then at 28°C) before electrophysiology experiments.

Sodium currents were recorded at room temperature in the whole-cell configuration of the patch-clamp technique (66) using an Axopatch 200B series amplifier (Molecular Devices). Whole-cell currents were acquired at 20 kHz and filtered at 5 kHz. Pulse generation and data collection were done with Clampex 9.2 (Molecular Devices). Bath solution contained 145 mM NaCl, 4 mM KCl, 1.8 mM $CaCl_2$, 1 mM $MgCl_2$, 10 mM HEPES, pH 7.35, and 310 mM mOsm/kg. TTX (150 nM) was present in the bath to block endogenous sodium currents. The composition of the pipette solution was as follows: 10 mM NaF, 110 mM CsF, 20 mM CsCl, 2 mM EGTA, 10 mM HEPES, pH 7.35, and 310 mOsm/kg. Osmolality and pH values were adjusted with sucrose and NaOH, respectively. Patch pipettes were pulled from thin-wall borosilicate glass (Warner Instruments) with a multistage P-97 Flaming-Brown Micropipette Puller (Sutter Instruments) and fire-polished with a Micro Forge MF 830 (Narashige). Pipette resistance was approximately 2 MΩ with standard recording solutions. Agar (2%) bridges containing bath solution served as reference electrodes.

Cells were allowed to equilibrate for 10 minutes in bath solution before obtaining seals. Peak currents were measured with pulses between –100 and +40 mV (10 s at the holding potential between pulses) from a holding potential of –120 mV. The peak current was normalized for cell capacitance and plotted against voltage to generate peak current density–voltage relationships. Whole-cell conductance was calculated from the peak current amplitude using the formula: $G_{Na} = I_{Na}/V - E_{rev}$, where G_{Na} is sodium conductance, I_{Na} is sodium current measured at test potential V, E_{rev} is the estimated Na^+ reversal potential, and then normalized to the maximal conductance recorded between –100 and 0 mV.

The voltage dependence of activation was calculated by fitting the normalized G-V curves with a Boltzmann function. The voltage dependence of channel availability was assessed following a 300-msec prepulse to various potentials and normalizing to the current measured following a pulse to –40 mV (membrane held for 20 s at the holding potential between pulses). The normalized G-V curves were fit with the Boltzmann function: $G = 1/(1 + \exp[V - V_{1/2}]/k)$ to determine the $V_{1/2}$ and slope factor (k).

Isolation and transfection of primary sensory neurons. DRGs from 4- to 6-week-old female and male Sprague-Dawley rats were harvested and dissociated as described previously (67). Briefly, DRG neurons were dissociated with a 20-minute incubation in 1.5 mg/ml collagenase A (Roche) and 0.6 mM EDTA, followed by an 18-minute incubation in 1.5 mg/ml collagenase D (Roche), 0.6 mM EDTA, and 30 U/ml papain (Worthington Biochemical Corp.). DRGs were then centrifuged and triturated in 0.5 ml of media containing 1.5 mg/ml BSA (low endotoxin) and 1.5 mg/ml trypsin inhibitor (Sigma-Aldrich). After trituration, 2 ml of DRG media were added to the cell suspension, which was filtered through a 70-μm nylon mesh cell strainer (BD Technologies). The mesh was washed twice with 2 ml of DRG media. The cells were then cotransfected with WT or mutant human $Na_V1.9$ plasmids and a plasmid encoding GFP using a Nucleofector IIS (Lonza) and an Amaxa Basic Neuron SCN Nucleofector Kit (VSPI-1003). Briefly, the cell suspension was centrifuged (100 ×*g* for 3 min), and the cell pellet was resuspended in 20 μl Nucleofector solution, mixed with 2 μg WT, L1302F, or L811P $Na_V1.9$ plasmid plus 0.2 μg GFP plasmid, and transfected using Nucleofector IIS and protocol SCN-BNP 6. After transfection, cells were allowed to recover in calcium-free DMEM, fed with DRG media supplemented with nerve growth

factor (50 ng/ml) and glial cell line–derived neurotrophic factor (50 ng/ml), and maintained at 37°C with 5% CO_2 for 40 to 55 hours before current-clamp recording. Recordings were obtained from nontransfected adult rat DRG neurons within 8 hours of isolation.

Current-clamp electrophysiology. The pipette solution contained the following: 140 mM KCl, 0.5 mM EGTA, 5 mM HEPES, 3 mM Mg-ATP, and 10 mM dextrose, pH 7.30, with KOH (adjusted to 310 mOsm with sucrose). The bath solution contained the following: 140 mM NaCl, 3 mM KCl, 2 mM $MgCl_2$, 2 mM $CaCl_2$, 10 mM HEPES, and 10 mM dextrose, pH 7.30, with NaOH (adjusted to 320 mOsm with sucrose). A whole-cell configuration was obtained in voltage-clamp mode before proceeding to the current-clamp recording mode. The electrophysiologist was blinded with respect to exogenous sodium channel expression in DRG neurons (either WT or mutant $Na_V1.9$) until after data analysis. Small DRG neurons with a diameter of less than 30 μm and green fluorescence were selected for recording. A stable (<10% variation) RMP for 30 seconds and the presence of endogenous $Na_V1.8$ currents (>1 nA) evaluated by holding neurons at –50 mV were used as additional criteria for inclusion. Input resistance was determined by the slope of a linear fit to hyperpolarizing responses to current steps from –5 pA to –40 pA in 5-pA increments. The minimum current injection required to achieve firing of a single action potential (designated as the current threshold) was determined at the first action potential elicited by a series of depolarizing current injections (200 ms) applied in 5-pA increments. Action potential amplitude was measured by the spike height from the peak to the RMP. Spontaneously firing cells were excluded from the analysis of RMP, input resistance, and action potential amplitude.

Statistics. Voltage-clamp data were analyzed and plotted using a combination of Clampfit 9.2 (Molecular Devices), SigmaPlot 12.5 (Systat Software), and Origin 7.0 (OriginLab). Statistical analyses were carried out using the statistical analysis option in SigmaPlot. Current-clamp data were analyzed using Fitmaster (HEKA Elektronik) and Origin (Microcal Software) software. Percentages of nonfiring cells and spontaneously firing cells were compared using the *z* test. Unless otherwise noted, statistical significance was determined using an independent 2-tailed *t* test. All electrophysiology data are presented as the mean ± SEM, and error bars in the figures represent the SEM. The number of cells (*n*) used for each experimental condition is indicated in the figures, figure legends, or tables. A *P* value of less than 0.05 was considered significant.

Study approval. The human study was approved by an independent ethics review board (protocol CIP-SEQ-001; Quorum Review, Inc., Seattle, WA, USA), and the proband provided written informed consent for participation and publication of the findings. Animal use was approved by the IACUC of the Veterans Administration West Haven Hospital.

Author contributions

JH, CGV, AC, and YPG performed experiments, collected and analyzed data, and contributed to the writing of the manuscript; SDDH, CJC, SGW, and ALG designed the study, evaluated results, and wrote the manuscript.

Acknowledgments

The authors thank Dayna Nevay, Emma Leach, Chris Radomski, and Julie MacFarlane (Xenon Pharmaceuticals, Inc.) for help with phenotype ascertainment and molecular genetics and Shujun Liu, Fadia Dib-Hajj, and Palak Shah (Yale University) for their technical assistance with this project. This work was supported by grants from the NIH (NS032387, to ALG); the Northwestern Medicine Catalyst Fund (to CGV and ALG); the Rehabilitation Research and Development Service and Medical Research Service of the Department of Veterans Affairs (to SGW); and the Erythromelalgia Association (to SGW). The Center for Neuroscience and Regeneration Research is a collaboration of the Paralyzed Veterans of America with Yale University.

Address correspondence to: Alfred L. George Jr., Department of Pharmacology, Northwestern University Feinberg School of Medicine, 320 East Superior Street, Chicago, Illinois 60611, USA. Phone: 312.503.4893; E-mail: al.george@northwestern.edu. Or to: Stephen G. Waxman, Neurorehabilitation Research Center, Veterans Affairs Hospital, 950 Campbell Ave, Building 34, West Haven, Connecticut 06516, USA. Phone: 203.668.1141; Email: stephen.waxman@yale.edu.

1. Dib-Hajj SD, Cummins TR, Black JA, Waxman SG. Sodium channels in normal and pathological pain. *Annu Rev Neurosci*. 2010;33:325–347.
2. Dib-Hajj SD, Yang Y, Black JA, Waxman SG. The Na(V)1.7 sodium channel: from molecule to man. *Nat Rev Neurosci*. 2013;14(1):49–62.
3. Dib-Hajj SD, Black JA, Waxman SG. NaV1.9: a sodium channel linked to human pain. *Nat Rev Neurosci*. 2015;16(9):511–519.
4. Liu M, Wood JN. The roles of sodium channels in nociception: implications for mechanisms of neuropathic pain. *Pain Med*. 2011;12 Suppl 3:S93–S99.
5. Bennett DL, Woods CG. Painful and painless channelopathies. *Lancet Neurol*. 2014;13(6):587–599.
6. Han C, Huang J, Waxman SG. Sodium channel Nav1.8: Emerging links to human disease. *Neurology*. 2016;86(5):473–483.
7. Dib-Hajj SD, Tyrrell L, Black JA, Waxman SG. NaN, a novel voltage-gated Na channel, is expressed preferentially in peripheral sensory neurons and down-regulated after axotomy. *Proc Natl Acad Sci U S A*. 1998;95(15):8963–8968.
8. Tate S, et al. Two sodium channels contribute to the TTX-R sodium current in primary sensory neurons. *Nat Neurosci*. 1998;1(8):653–655.
9. Akopian AN, et al. The tetrodotoxin-resistant sodium channel SNS has a specialized function in pain pathways. *Nat Neurosci*. 1999;2(6):541–548.
10. Persson AK, Black JA, Gasser A, Cheng X, Fischer TZ, Waxman SG. Sodium-calcium exchanger and multiple sodium channel isoforms in intra-epidermal nerve terminals. *Mol Pain*. 2010;6:84.
11. Cummins TR, Dib-Hajj SD, Black JA, Akopian AN, Wood JN, Waxman SG. A novel persistent tetrodotoxin-resistant sodium current in SNS-null and wild-type small primary sensory neurons. *J Neurosci*. 1999;19(24):RC43.
12. Dib-Hajj SD, Tyrrell L, Escayg A, Wood PM, Meisler MH, Waxman SG. Coding sequence, genomic organization, and conserved chromosomal localization of the mouse gene Scn11a encoding the sodium channel NaN. *Genomics*. 1999;59(3):309–318.
13. Fang X, Djouhri L, Black JA, Dib-Hajj SD, Waxman SG, Lawson SN. The presence and role of the tetrodotoxin-resistant sodium channel Na(v)1.9 (NaN) in nociceptive primary afferent neurons. *J Neurosci*. 2002;22(17):7425–7433.
14. Ostman JA, Nassar MA, Wood JN, Baker MD. GTP up-regulated persistent Na+ current and enhanced nociceptor excitability require NaV1.9. *J Physiol (Lond)*. 2008;586(4):1077–1087.
15. Baker MD, Chandra SY, Ding Y, Waxman SG, Wood JN. GTP-induced tetrodotoxin-resistant Na+ current regulates excitability in mouse and rat small diameter sensory neurones. *J Physiol (Lond)*. 2003;548(Pt 2):373–382.
16. Lai J, Porreca F, Hunter JC, Gold MS. Voltage-gated sodium channels and hyperalgesia. *Annu Rev Pharmacol Toxicol*. 2004;44:371–397.
17. Priest BT, et al. Contribution of the tetrodotoxin-resistant voltage-gated sodium channel NaV1.9 to sensory transmission and nociceptive behavior. *Proc Natl Acad Sci U S A*. 2005;102(26):9382–9387.

18. Amaya F, et al. The voltage-gated sodium channel Na(v)1.9 is an effector of peripheral inflammatory pain hypersensitivity. *J Neurosci*. 2006;26(50):12852–12860.
19. Hoffmann T, Kistner K, Carr RW, Nassar MA, Reeh PW, Weidner C. Reduced excitability and impaired nociception in peripheral unmyelinated fibers from Nav1.9-null mice. *Pain*. 2017;158(1):58–67.
20. Dib-Hajj S, Black JA, Cummins TR, Waxman SG. NaN/Nav1.9: a sodium channel with unique properties. *Trends Neurosci*. 2002;25(5):253–259.
21. Coste B, Osorio N, Padilla F, Crest M, Delmas P. Gating and modulation of presumptive NaV1.9 channels in enteric and spinal sensory neurons. *Mol Cell Neurosci*. 2004;26(1):123–134.
22. Vanoye CG, Kunic JD, Ehring GR, George AL. Mechanism of sodium channel NaV1.9 potentiation by G-protein signaling. *J Gen Physiol*. 2013;141(2):193–202.
23. Herzog RI, Cummins TR, Waxman SG. Persistent TTX-resistant Na+ current affects resting potential and response to depolarization in simulated spinal sensory neurons. *J Neurophysiol*. 2001;86(3):1351–1364.
24. Lin Z, Santos S, Padilla K, Printzenhoff D, Castle NA. Biophysical and Pharmacological Characterization of Nav1.9 Voltage Dependent Sodium Channels Stably Expressed in HEK-293 Cells. *PLoS One*. 2016;11(8):e0161450.
25. Han C, et al. The Domain II S4-S5 Linker in Nav1.9: A Missense Mutation Enhances Activation, Impairs Fast Inactivation, and Produces Human Painful Neuropathy. *Neuromolecular Med*. 2015;17(2):158–169.
26. Leipold E, et al. A de novo gain-of-function mutation in SCN11A causes loss of pain perception. *Nat Genet*. 2013;45(11):1399–1404.
27. Huang J, et al. Small-fiber neuropathy Nav1.8 mutation shifts activation to hyperpolarized potentials and increases excitability of dorsal root ganglion neurons. *J Neurosci*. 2013;33(35):14087–14097.
28. Faber CG, et al. Gain-of-function Nav1.8 mutations in painful neuropathy. *Proc Natl Acad Sci U S A*. 2012;109(47):19444–19449.
29. Gingras J, et al. Global Nav1.7 knockout mice recapitulate the phenotype of human congenital indifference to pain. *PLoS One*. 2014;9(9):e105895.
30. Alexandrou AJ, et al. Subtype-selective small molecule inhibitors reveal a fundamental role for Nav1.7 in nociceptor electrogenesis, axonal conduction and presynaptic release. *PLoS One*. 2016;11(4):e0152405.
31. Woods CG, Babiker MO, Horrocks I, Tolmie J, Kurth I. The phenotype of congenital insensitivity to pain due to the NaV1.9 variant p.L811P. *Eur J Hum Genet*. 2015;23(5):561–563.
32. Phatarakijnirund V, et al. Congenital insensitivity to pain: Fracturing without apparent skeletal pathobiology caused by an autosomal dominant, second mutation in SCN11A encoding voltage-gated sodium channel 1.9. *Bone*. 2016;84:289–298.
33. Zhang XY, et al. Gain-of-function mutations in SCN11A cause familial episodic pain. *Am J Hum Genet*. 2013;93(5):957–966.
34. Huang J, et al. Gain-of-function mutations in sodium channel Na(v)1.9 in painful neuropathy. *Brain*. 2014;137(Pt 6):1627–1642.
35. Leipold E, et al. Cold-aggravated pain in humans caused by a hyperactive NaV1.9 channel mutant. *Nat Commun*. 2015;6:10049.
36. Okuda H, et al. Infantile Pain Episodes Associated with Novel Nav1.9 Mutations in Familial Episodic Pain Syndrome in Japanese Families. *PLoS One*. 2016;11(5):e0154827.
37. Han C, et al. Familial gain-of-function Nav1.9 mutation in a painful channelopathy. *J Neurol Neurosurg Psychiatr*. 2017;88(3):233–240.
38. Landrieu P, Said G, Allaire C. Dominantly transmitted congenital indifference to pain. *Ann Neurol*. 1990;27(5):574–578.
39. Goldberg YP, et al. Loss-of-function mutations in the Nav1.7 gene underlie congenital indifference to pain in multiple human populations. *Clin Genet*. 2007;71(4):311–319.
40. Nilsen KB, Nicholas AK, Woods CG, Mellgren SI, Nebuchennykh M, Aasly J. Two novel SCN9A mutations causing insensitivity to pain. *Pain*. 2009;143(1-2):155–158.
41. Baker MD, Chandra SY, Ding Y, Waxman SG, Wood JN. GTP-induced tetrodotoxin-resistant Na+ current regulates excitability in mouse and rat small diameter sensory neurones. *J Physiol (Lond)*. 2003;548(Pt 2):373–382.
42. Renganathan M, Cummins TR, Waxman SG. Contribution of Na(v)1.8 sodium channels to action potential electrogenesis in DRG neurons. *J Neurophysiol*. 2001;86(2):629–640.
43. Patrick Harty T, Waxman SG. Inactivation properties of sodium channel Nav1.8 maintain action potential amplitude in small DRG neurons in the context of depolarization. *Mol Pain*. 2007;3:12.
44. Kocsis JD, Waxman SG. Intra-axonal recordings in rat dorsal column axons: membrane hyperpolarization and decreased excitability precede the primary afferent depolarization. *Brain Res*. 1982;238(1):222–227.
45. Waxman SG. Neurobiology: a channel sets the gain on pain. *Nature*. 2006;444(7121):831–832.
46. Vasylyev DV, Han C, Zhao P, Dib-Hajj S, Waxman SG. Dynamic-clamp analysis of wild-type human Nav1.7 and erythromelalgia mutant channel L858H. *J Neurophysiol*. 2014;111(7):1429–1443.
47. Cox JJ, et al. An SCN9A channelopathy causes congenital inability to experience pain. *Nature*. 2006;444(7121):894–898.
48. Ahmad S, et al. A stop codon mutation in SCN9A causes lack of pain sensation. *Hum Mol Genet*. 2007;16(17):2114–2121.
49. Dib-Hajj SD, et al. Gain-of-function mutation in Nav1.7 in familial erythromelalgia induces bursting of sensory neurons. *Brain*. 2005;128(Pt 8):1847–1854.
50. Han C, et al. Functional profiles of SCN9A variants in dorsal root ganglion neurons and superior cervical ganglion neurons correlate with autonomic symptoms in small fibre neuropathy. *Brain*. 2012;135(Pt 9):2613–2628.
51. Han C, et al. Temperature dependence of erythromelalgia mutation L858F in sodium channel Nav1.7. *Mol Pain*. 2007;3:3.
52. Cummins TR, Dib-Hajj SD, Waxman SG. Electrophysiological properties of mutant Nav1.7 sodium channels in a painful inherited neuropathy. *J Neurosci*. 2004;24(38):8232–8236.
53. Rush AM, Dib-Hajj SD, Liu S, Cummins TR, Black JA, Waxman SG. A single sodium channel mutation produces hyper- or hypoexcitability in different types of neurons. *Proc Natl Acad Sci U S A*. 2006;103(21):8245–8250.
54. Han C, et al. Early- and late-onset inherited erythromelalgia: genotype-phenotype correlation. *Brain*. 2009;132(Pt 7):1711–1722.
55. Huang J, et al. Depolarized inactivation overcomes impaired activation to produce DRG neuron hyperexcitability in a Nav1.7 mutation in a patient with distal limb pain. *J Neurosci*. 2014;34(37):12328–12340.
56. Renganathan M, Gelderblom M, Black JA, Waxman SG. Expression of Nav1.8 sodium channels perturbs the firing patterns of cerebellar Purkinje cells. *Brain Res*. 2003;959(2):235–242.
57. Cannon SC. Pathomechanisms in channelopathies of skeletal muscle and brain. *Annu Rev Neurosci*. 2006;29:387–415.
58. George AL. Inherited disorders of voltage-gated sodium channels. *J Clin Invest*. 2005;115(8):1990–1999.
59. Cannon SC, Strittmatter SM. Functional expression of sodium channel mutations identified in families with periodic paralysis. *Neuron*. 1993;10(2):317–326.
60. Yang N, et al. Sodium channel mutations in paramyotonia congenita exhibit similar biophysical phenotypes in vitro. *Proc Natl Acad Sci U S A*. 1994;91(26):12785–12789.
61. Sokolov S, Scheuer T, Catterall WA. Gating pore current in an inherited ion channelopathy. *Nature*. 2007;446(7131):76–78.
62. Struyk AF, Cannon SC. A Na+ channel mutation linked to hypokalemic periodic paralysis exposes a proton-selective gating pore. *J Gen Physiol*. 2007;130(1):11–20.
63. Wilson MH, Coates CJ, George AL. PiggyBac transposon-mediated gene transfer in human cells. *Mol Ther*. 2007;15(1):139–145.
64. Kahlig KM, Saridey SK, Kaja A, Daniels MA, George AL, Wilson MH. Multiplexed transposon-mediated stable gene transfer in human cells. *Proc Natl Acad Sci U S A*. 2010;107(4):1343–1348.
65. Yusa K, Zhou L, Li MA, Bradley A, Craig NL. A hyperactive piggyBac transposase for mammalian applications. *Proc Natl Acad Sci U S A*. 2011;108(4):1531–1536.
66. Hamill OP, Marty A, Neher E, Sakmann B, Sigworth FJ. Improved patch-clamp techniques for high-resolution current recording from cells and cell-free membrane patches. *Pflugers Arch*. 1981;391(2):85–100.
67. Dib-Hajj SD, et al. Transfection of rat or mouse neurons by biolistics or electroporation. *Nat Protoc*. 2009;4(8):1118–1126.